NT3-chitosan enables de novo regeneration and functional recovery in monkeys after spinal cord injury

Jia-Sheng Rao[a,b,c,1], Can Zhao[b,a,c,1], Aifeng Zhang[d,1], Hongmei Duan[e,1], Peng Hao[e,1], Rui-Han Wei[a,1], Junkui Shang[e,1], Wen Zhao[e], Zuxiang Liu[f,g,h], Juehua Yu[i], Kevin S. Fan[j], Zhaolong Tian[k], Qihua He[l], Wei Song[m], Zhaoyang Yang[e,b,2], Yi Eve Sun[i,n,2], and Xiaoguang Li[e,b,a,2]

[a]Beijing Key Laboratory for Biomaterials and Neural Regeneration, School of Biological Science and Medical Engineering, Beihang University, 100083 Beijing, China; [b]Beijing International Cooperation Bases for Science and Technology on Biomaterials and Neural Regeneration, Beijing Advanced Innovation Center for Big Data-Based Precision Medicine, Beihang University, 100083 Beijing, China; [c]Beijing Advanced Innovation Center for Biomedical Engineering, Beihang University, 100083 Beijing, China; [d]Beijing Friendship Hospital, Capital Medical University, 100068 Beijing, China; [e]Department of Neurobiology, School of Basic Medical Sciences, Capital Medical University, 100069 Beijing, China; [f]State Key Laboratory of Brain and Cognitive Science, Institute of Biophysics, Chinese Academy of Sciences, 100101 Beijing, China; [g]Innovation Center of Excellence on Brain Science, Chinese Academy of Sciences, 100101 Beijing, China; [h]Department of Biology, College of Life Sciences, University of Chinese Academy of Sciences, 100049 Beijing, China; [i]Translational Stem Cell Research Center, Tongji Hospital, Tongji University School of Medicine, 200065 Shanghai, China; [j]Department of Computer Engineering, University of California, Santa Barbara, CA 93106; [k]Department of Anesthesiology, Xuanwu Hospital Capital Medical University, 100053 Beijing, China; [l]Centre of Medical and Health Analysis, Peking University Health Science Center, 100191 Beijing, China; [m]Rehabilitation Engineering Research Institute, China Rehabilitation Research Center, 100068 Beijing, China; and [n]Department of Psychiatry and Biobehavioral Sciences, UCLA Medical School, Los Angeles, CA 90095

Edited by Nancy Y. Ip, The Hong Kong University of Science and Technology, Hong Kong, China, and approved April 30, 2018 (received for review March 20, 2018)

Spinal cord injury (SCI) often leads to permanent loss of motor, sensory, and autonomic functions. We have previously shown that neurotrophin3 (NT3)-loaded chitosan biodegradable material allowed for prolonged slow release of NT3 for 14 weeks under physiological conditions. Here we report that NT3-loaded chitosan, when inserted into a 1-cm gap of hemisectioned and excised adult rhesus monkey thoracic spinal cord, elicited robust axonal regeneration. Labeling of cortical motor neurons indicated motor axons in the corticospinal tract not only entered the injury site within the biomaterial but also grew across the 1-cm-long lesion area and into the distal spinal cord. Through a combination of magnetic resonance diffusion tensor imaging, functional MRI, electrophysiology, and kinematics-based quantitative walking behavioral analyses, we demonstrated that NT3-chitosan enabled robust neural regeneration accompanied by motor and sensory functional recovery. Given that monkeys and humans share similar genetics and physiology, our method is likely translatable to human SCI repair.

nonhuman primate | spinal cord injury repair | chitosan | NT3 | CST regeneration

Neurons in the central nervous system (CNS) do not regenerate, not only because their innate regeneration potential is attenuated compared with neurons in the peripheral nervous system but also due to the hostile CNS injury environment composed of inhibitory myelin debris (1–3), extracellular matrix molecules including chondroitin sulfate proteoglycans (CSPGs) (4, 5), as well as inflammatory cytokines (6, 7), which further dampen the regeneration process. As a result, spinal cord injury (SCI) often leads to permanent motor, sensory, and autonomic functional loss. Previous attempts were made through local applications of neurotrophic factors (8–11), transplantation of exogenous neural stem cells (12, 13), Schwann cells (14, 15), peripheral nerve grafts (16, 17), chondroitinase ABC (18, 19), knocking out the CSPG receptor (20), and usage of biomaterials (10, 21–24) to provide an optimal microenvironment for neural repair in rodent SCI models. Measurable improvement in axonal regeneration and functional recoveries had been observed. However, studies using rodent models may not be translatable to humans because of quite dramatic differences in the genome (similarity between the rodent and human genomes is only around 80%), immune system development and function, and certainly the structure and function of the CNS (25, 26). Therefore, in the drug development field, it has been well-acknowledged that an overwhelmingly large number of drugs that cured mouse diseases ended up failing in clinical trials (25). SCI research using nonhuman primate (NHP) models, on the other hand, has been rather limited (27–31). Some of the interventions tested in monkeys were relevant to clinical settings, such as application of localized cooling (hypothermia) to reduce edema and inflammation to curb secondary lesions (32). In recent years, the use of trophic factors (33), antibodies (34–36), and transplantation of neural stem cells (37, 38) to promote regeneration has attracted a lot of attention in NHP SCI research; however, whether these methods could in the future be applicable to human SCI repair is yet to be investigated. In addition, although peripheral nerve (39, 40) or other biocompatible scaffolds (40) had been examined and proposed for clinical applications, positive clinical trial results remain to be seen.

Significance

Spinal cord injury (SCI) is a severe medical condition often leading to permanent loss of sensory, motor, and autonomic functions, currently with no cure. This study provides evidence that in monkeys with severe SCI, a bioactive and biodegradable material, NT3-chitosan, elicited robust de novo neural regeneration including, for example, long-distance axonal growth of cortical motor neurons in the cortical spinal tract, as well as sensory and motor functional recovery. In this study, we utilized a battery of minimally invasive outcome measures including fMRI, magnetic resonance diffusion tensor imaging, and kinematics walking analyses, which are all clinical trial-compatible. Essentially, success in this approach in nonhuman primate SCI models provides a solid foundation for its potential therapeutic application.

Author contributions: J.S.R., C.Z., A.Z., H.D., P.H., R.H.W., Z.Y., Y.E.S., and X.L. designed research; J.S.R., C.Z., A.Z., H.D., P.H., R.H.W., J.S., W.Z., Z.L., Z.T., W.S., Z.Y., and X.L. performed research; Z.L. and Q.H. contributed new reagents/analytic tools; J.S.R., C.Z., H.D., P.H., R.H.W., J.S., W.Z., J.Y., K.S.F., Z.Y., and Y.E.S. analyzed data; and J.S.R., C.Z., H.D., P.H., J.S., Z.Y., Y.E.S., and X.L. wrote the paper.

The authors declare no conflict of interest.

This article is a PNAS Direct Submission.

[1]J.S.R., C.Z., A.Z., H.D., P.H., R.H.W., and J.S. contributed equally to this work.

[2]To whom correspondence may be addressed. Email: wack_lily@163.com, yi.eve.sun@gmail.com, or lxgchina@sina.com.

This article contains supporting information online at www.pnas.org/lookup/suppl/doi:10.1073/pnas.1804735115/-/DCSupplemental.

We used chitosan to serve as a matrix scaffold to load neurotrophin3 (NT3) so that this critical neurotrophic factor could be gradually and continuously released into the milieu after implantation, in a relatively long term manner. Our NT3-chitosan allowed for controlled release of NT3 at 37 °C when cocultured with neural stem cells (NSCs) for at least 14 wk (10). In rodent SCI models, the NT3-chitosan scaffold effectively prevented infiltration of inflammatory cells and attracted endogenous NSCs to proliferate, migrate, and differentiate into neurons, forming nascent relay neuronal networks to transmit ascending and descending neural signals to proper targets (41, 42). In addition, NT3-chitosan also promoted robust axonal regeneration (22, 41, 42). In this study, which is one step closer to human clinical trials, we developed a rhesus monkey spinal cord hemisection and extraction SCI model leaving a 1-cm gap, which was either left alone (lesion control) or inserted with NT3-chitosan material (NT3-chitosan). Since, from rodent studies, we found that either the chitosan scaffold alone or chitosan scaffold plus chitosan matrix without NT3 only elicited an antiinflammatory effect in preventing immune cell infiltration into the control chitosan material without attracting NSC infiltration and did not enable neural regeneration, we omitted such control groups in this monkey study for ethical concerns regarding excessive use of NHPs. Using biotinylated dextran amine (BDA) injection to label cortical motor neurons, we tracked the corticospinal tract (CST) and discovered that regenerated axons entered the lesion area into the bioscaffold, grew across the 1-cm-long lesion area, and extended into the distal spinal cord. In addition, a combination of minimally invasive functional magnetic resonance imaging (fMRI), diffusion tensor imaging (DTI), electrophysiology, and kinematics walking behavioral analyses indicated neural regeneration as well as substantial motor and sensory functional recovery in the NT3-chitosan group. Quantitative outcome measures clearly demonstrated significant differences between the lesion control and NT3-chitosan groups. The bioactive material is antiinflammatory and growth-promoting with no risk of tumor formation (compared with exogenous NSC-based therapies). Success in this approach in NHP-SCI models provides a solid foundation for its potential therapeutic application.

Results

Morphological Analyses Demonstrating NT3-Chitosan Elicited Robust Axonal Regeneration. In our previous studies using rodents, complete spinal cord transection and segment removal were used (42). However, due to animal care concerns, complete spinal cord transection in monkeys was avoided due to high instances of mortality (40, 26). Thirty-two animals were subjected to spinal cord hemisection at thoracic level T8 (the eighth vertebral bone) followed by removal of a 1-cm segment of the right half of the spinal cord (Fig. 1*A*). A 1-cm-long NT3-chitosan matrix in a tubular scaffold was inserted individually into the lesion gap of 20 animals, and the remaining 12 animals were used as lesion controls. Suturing of the dura was performed to protect the lesion site. Another six animals without SCI were used as non-injury controls. All information on each of the animals used in the study regarding the occurrence of bedsores, time of death post surgery, cause of death, and types of analyses performed is listed in *SI Appendix*, Tables S1–S3. We are fully aware that such an extreme injury condition almost never happens in human SCI in the clinic; however, to demonstrate the superb de novo neural regeneration, namely generation of connecting neural tissue from an empty space, we chose this extreme model. We will discuss the clinical implications of our study later in the article.

Interestingly, bedsores, a clinically relevant outcome following SCI, also frequently happen in monkeys after SCI (43). NT3-chitosan significantly reduced the incidence of bedsores, with a 58.3% occurrence rate in the lesion control group and reduced to 10.5% in the NT3-chitosan group, which could be indicative of better SCI recovery. At gross anatomical levels, over 1 y after the surgery, a neural cable-like "bridging" structure connecting the rostral and caudal ends of the severed right side of the spinal cord appeared in the NT3-chitosan matrix, whereas only scar tissues were found in the lesion control group (Fig. 1 *A* and *B*). In *SI Appendix*, Fig. S1, gross anatomy of regenerated monkey spinal cord from five additional animals is shown, and lesion size of each of the 32 SCI animals going through the injury operation is listed, indicative of consistent lesion operations and similar sizes of lesion areas. In fact, the surgical team performed the hemisection before knowing the subsequent lesion control (LC) or NT3-chitosan (NT3) group assignment, which added more objectivity to the design of the study. This de novo regenerated tissue shared stark similarity in gross anatomical appearance with NT3-chitosan–elicited de novo regeneration of rat neural tissues after complete SCI (Fig. 1*B*, *Right*) (42). Moreover, immunohistological and electron microscopic analyses demonstrated that the cable-like regenerated neural tissues contained many myelinated and neurofilament (NF)-positive nerve fibers (Fig. 1 *C* and *D* and *SI Appendix*, Table S4). Moreover, many cell bodies aligned well along the anterior–posterior axis, which could be NF-positive neuronal cells (Fig. 1*C*). H&E staining and NF staining on regenerated tissues at 11, 15, and 24 mo post operation (*SI Appendix*, Figs. S2 and S3) demonstrated that when axons or cell bodies encountered chitosan particles, they detour around and extend or migrate only in spaces between particles, making axon tracks difficult to see (*SI Appendix*, Figs. S2 and S3). However, after chitosan particles disappeared (degraded), relatively more longitudinally oriented fibers could be observed. The two-end funnel-like structures made tracking of axons difficult, especially at the two funnel ends. As the axons likely curve in and out of the section plane, it would appear that they suddenly were disrupted (*SI Appendix*, Figs. S2 and S3). In the LC group, although some levels of neural tissue invasion from the uninjured part of the spinal cord were apparent, major portions of the lesion area were filled with scarring cells that were NF-negative, and no myelinated axons were detected (Fig. 1 *C* and *D*). In some cases, watery cysts may form in the LC group, which after perfusion left a big empty space on the lesion side (Fig. 2*C*). In this monkey study, we found that GFAP-positive reactive astrocytes (*SI Appendix*, Fig. S4) and CD45-positive leukocytes and microglia (*SI Appendix*, Fig. S5) were substantially reduced with NT3-chitosan treatment, indicative of reduced inflammation and glial scar formation. As expected from our previous rat studies, revascularization occurred in regenerated neural tissues (*SI Appendix*, Fig. S5).

Robust Axonal Regeneration Elicited by NT3-Chitosan as Demonstrated by CST Tracking. To evaluate whether NT3-chitosan enabled long-distance axonal regeneration, we performed CST tracking using BDA. BDA was injected unilaterally into the motor cortex via a stereotactic method to achieve labeling of the CST over the years after the initial injury/transplantation operation. As shown in *SI Appendix*, Fig. S6, while no BDA signals could be detected about 15 mm distal to the caudal lesion edge in LC monkeys, plenty of BDA signals were detected in the expected column in the NT3 group (*SI Appendix*, Fig. S6*A*, *Right*). In addition, longitudinal sectioning of additional animals clearly demonstrated that regenerated CSTs grew through the GFAP-positive reactive astrocytic zone/barrier at the interface of the severed spinal cord and NT3-chitosan scaffold, entering the lesion/repaired area and then exiting the scaffold, and grew into the distal spinal cord (Fig. 2). These results demonstrate clear long-distance axonal regeneration.

Electrophysiological Results Indicating Partial Restoration After NT3-Chitosan Treatment. To examine whether NT3-chitosan also triggered sensory, particularly proprioception, recovery, we used Keypoint-II electromyography (Medtronic) to measure the somatosensory evoked potential (SEP) from both left and right anterior tibial muscles (Fig. 3). Proper signals were detected in the corresponding somatosensory cortex when either the left or the right tibial muscles

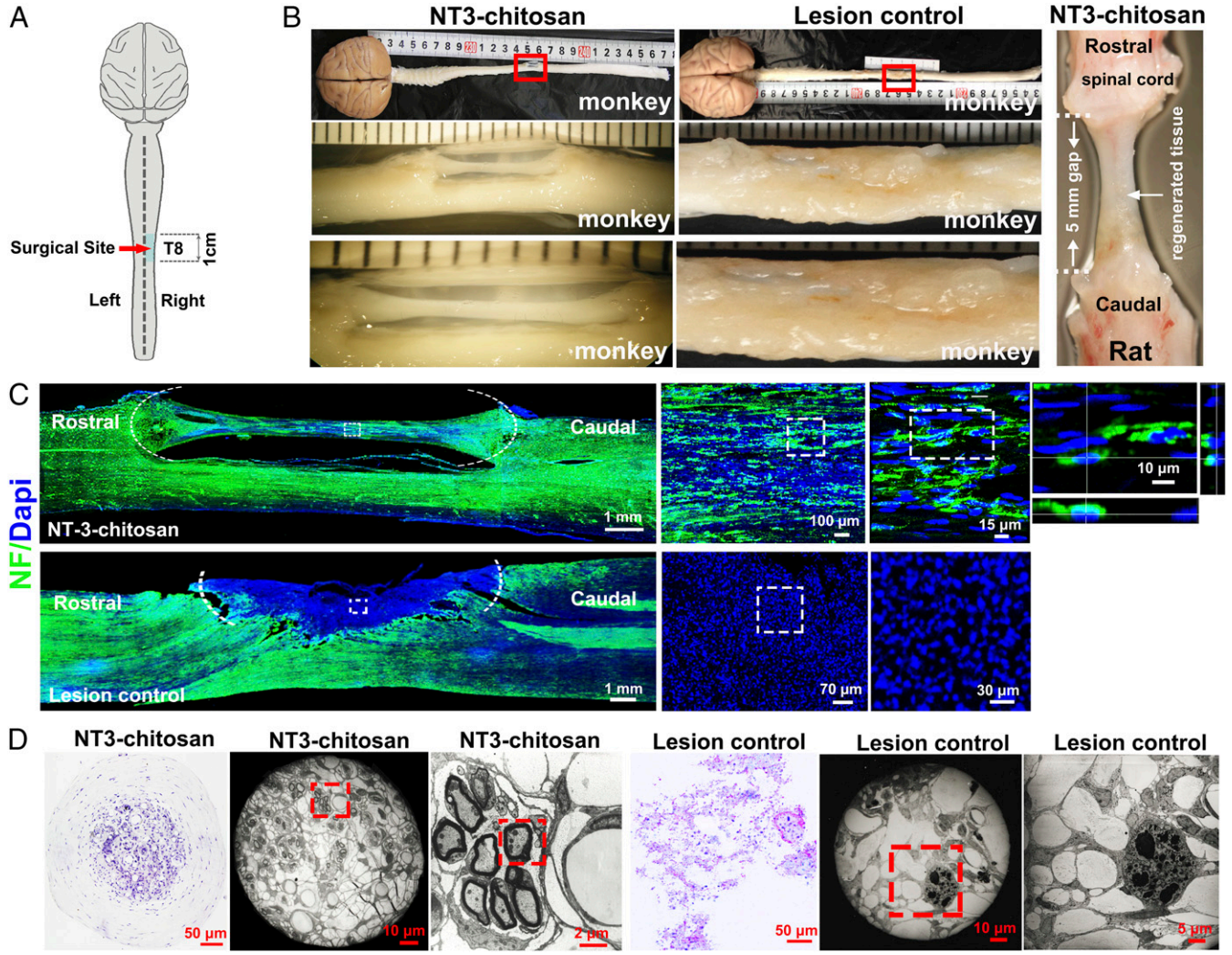

Fig. 1. Histological analyses demonstrating NT3-chitosan elicited de novo neural tissue reconstruction after a severe case of SCI. (*A*) A schema illustrating spinal cord hemisection and extraction leaving a 1-cm gap in monkey right spinal cord at thoracic level T8 (eighth vertebra), which was either left alone (lesion control) or inserted with NT3-chitosan matrix-containing tubular biomaterial (NT3-chitosan). (*B*) Gross anatomical analysis demonstrated regeneration of neural cable-like tissues in the NT3 group at the lesion/regeneration site, while only scar tissues filled the injury site in the LC group. (*B*, *Right*) NT3-chitosan–induced regeneration of neural cable-like structure in rat 9 mo after complete transection and extraction of rat thoracic spinal cord is shown. Results demonstrate the similarity between monkey and rat de novo regenerated neural tissues. (*C*) Immunofluorescent neurofilament staining (green) detected in regenerated neural tissues with NT3-chitosan treatment, while the LC group showed a lack of NF immunoreactivity in a major part of the lesion area. Quantitative measures of the bridge tissue diameter and the NF staining fiber density for the NT3 group are shown in *SI Appendix*, Table S4. (*D*) Over 24 mo after the operation, 1-mm-long spinal cord tissue was selected around the middle point of the regenerated tissue in the tube, and then semithin slices were made by staining with toluidine blue. The light micrographs show a large amount of regenerated blood vessels and myelinated and unmyelinated axons surrounded by epineurium- or perineurium-like structures in the regenerated cable tissue.

were stimulated in uninjured animals. In the LC group, no signals could be detected in the left or right somatosensory cortex when the right hind limb was stimulated. Interestingly, when the left hind limb was stimulated, SEP signals detected in the right cortex were reduced in the LC group compared with uninjured controls (Fig. 3). This was probably due to influence from injury to the right spinal cord, including inflammation, edema, demyelination, and so forth. As expected, in the NT3 group, clear SEP signals were detected in the left somatosensory cortex with stimulation of the right tibial muscle (Fig. 3). SEP signals in the right cortex when stimulating the left muscle were also greater than those in the LC group, indicative of better neural protection. To confirm that such SEP signals were not mediated by any kind of compensation from the intact left spinal cord, right after the initial SEP measurement we performed transection to the left spinal cord also at vertebral T8 followed by a 1-cm segment removal. Three months later, we found that retransection completely eliminated left hind limb-evoked SEP signals in the right cortex but did not ablate SEP signals detected in the left somatosensory cortex, which were evoked by stimulation of the right hind limb (Fig. 3). In contrast, when we recut the regenerated neural tissue on the right spinal cord, regained SEP signals in the left cortex completely disappeared after stimulation of the right hind limb. This observation suggested that the cortical–spinal connection through the injured right spinal cord was reestablished in the NT3-chitosan group.

In addition to SEP, we also measured motor evoked potential (MEP) (Fig. 4). Similar to sensory recovery, NT3-chitosan also triggered motor recovery as measured by MEP. It is worth mentioning that cortical motor axons have two branches. The main branch decussates the midline and continues down the spinal cord on the contralateral side. The minor branch does not decussate, and remains on the ipsilateral side. We examined responses from both the

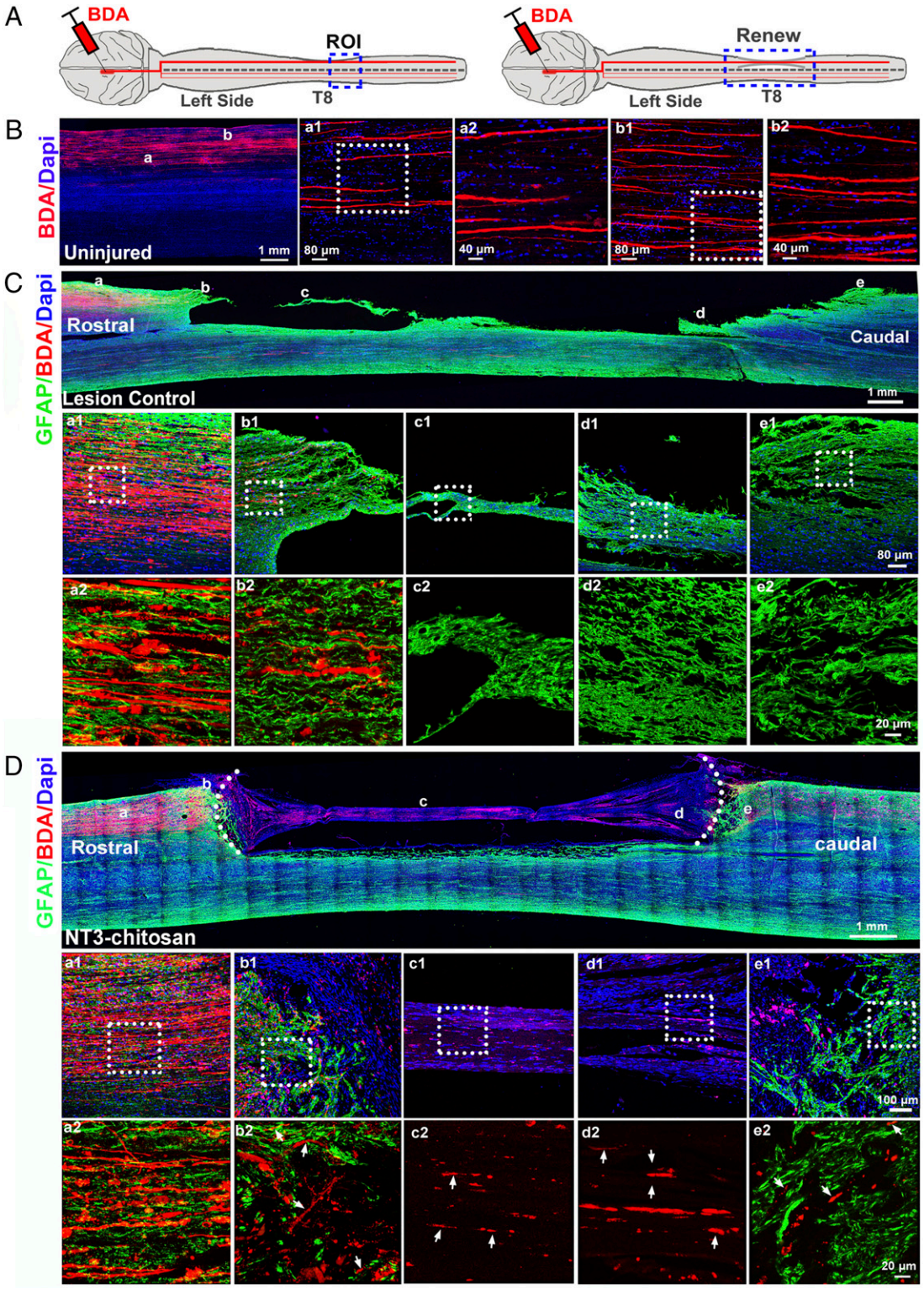

Fig. 2. CST tracking with unilateral BDA injections. (*A*) A diagram of BDA injections in uninjured and NT3-chitosan monkeys. (*B–D*) Longitudinal sections of monkey spinal cord 11 wk after BDA injections in normal (uninjured, animal 30) (*B*), lesion control (animal 5) (*C*), and NT3-chitosan (animal 18) (*D*) monkeys more than a year after the initial operation. DAPI (blue), BDA (red), and GFAP (green) fluorescent images are shown. ROI, region of interest; small white arrows marked regenerated BDA-positive fibers.

contralateral and ipsilateral sides when stimulating either left or right motor cortices. NT3-chitosan–triggered partial restoration of MEP signals was again not mediated by any sprouting or compensation from the intact left spinal cord but from de novo regenerated neural tissue in the right spinal cord, because 3 mo after second surgeries, the main (contralateral) MEP signals detected from the right hind limb persisted after transection of the left (intact) spinal cord and were abolished after retransection of the regenerated neural tissue

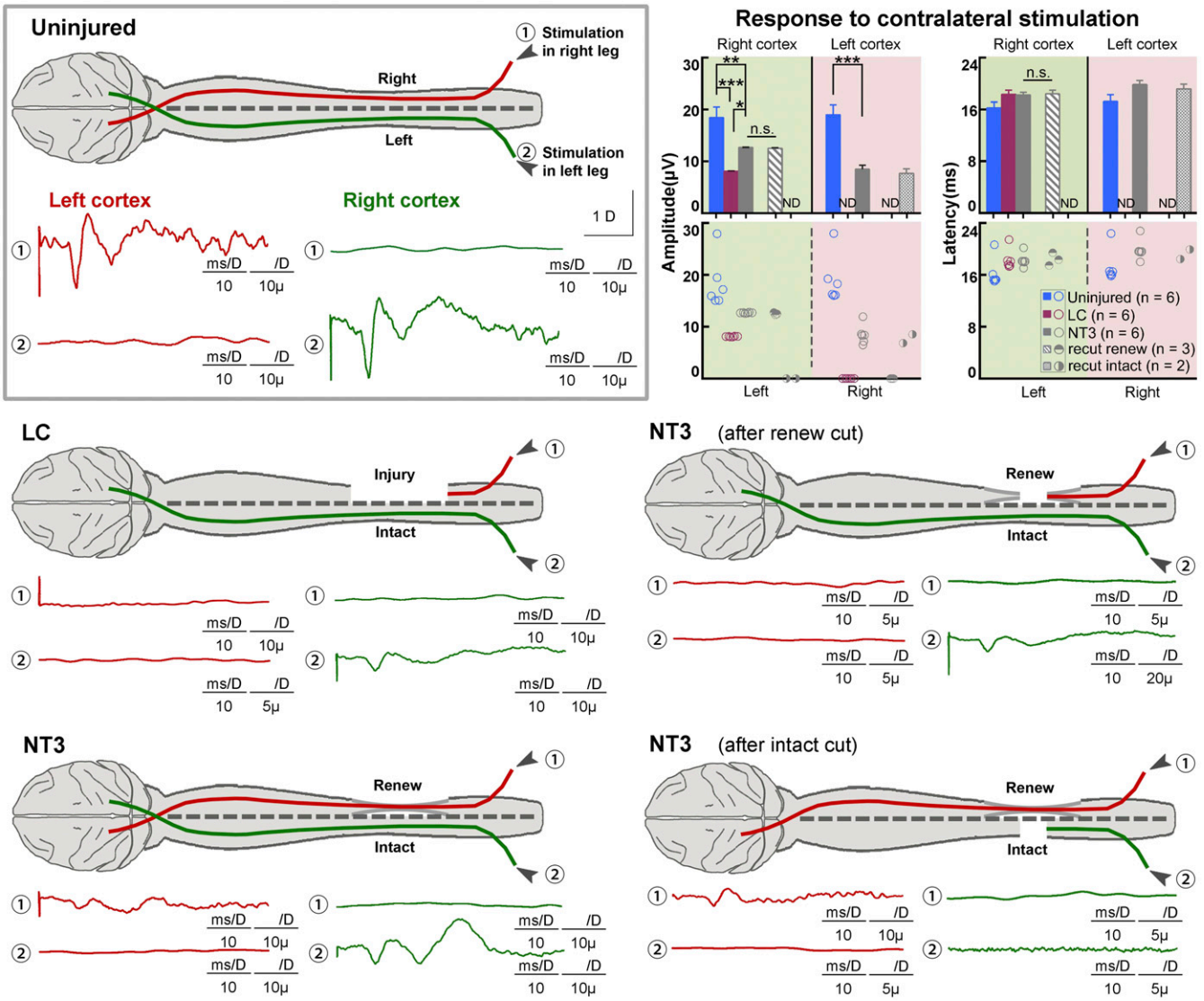

Fig. 3. SEPs demonstrating partial restorations with NT3-chitosan treatment. SEPs detected in left S1 (red) when right anterior tibial muscle was stimulated, and in right somatosensory cortex (green) when left hind limb muscle was stimulated, over 12 mo after the SCI operation. Lesion to the right spinal cord at T8 completely abolished SEP in left S1 cortex in the LC group, while it attenuated SEP signals in right S1, probably due to a spread of inflammation or secondary lesion. SEP reappeared in left S1 in the NT3 group; signals in the right S1 were also enhanced, likely due to the antiinflammatory effect of NT3-chitosan. In NT3 group animals, further lesion of the contralateral half (left) of the intact spinal cord completely abolished SEP signals in the right S1, while signals in the left S1 persisted. Resection of the regenerated neural cable, on the other hand, abolished SEP in left S1, and attenuated SEP signals in the right S1. Quantification and statistical analyses of amplitude and latency period for the aforementioned experiments are shown. Resection results of each animal are also displayed. Technical measurements were repeated twice. Shown are mean ± SEM. $*P < 0.05$, $**P < 0.01$, $***P < 0.001$ by ANOVA or two-tailed independent sample *t* test. ND, not determined; n.s., not significant. See *SI Appendix*, Tables S10 and S11 for exact *n* and *P* values.

(Fig. 4). Minor (ipsilateral) MEP signals also indicated that regenerated neural tissue was functional. Quantitative data of SEP and MEP amplitude and latency are presented (Figs. 3 and 4), both of which demonstrated partial but significant restoration with NT3-chitosan treatment. It is worth noting that the latencies of contralateral and ipsilateral MEPs in the NT3 group were longer (Fig. 4), which might indicate that the regenerated neural tissue had additional relay synapses or that newly regenerated axons were not fully myelinated for effective neurotransmission.

fMRI Analyses Indicating Recovery of Sensory Function with NT3-Chitosan Treatment. To establish additional outcome measures that are minimally invasive and can be used in clinical trials, we used fMRI to evaluate temperature sensation mediated by the spinothalamic tract. First, in uninjured animals, we used a laser stimulator to generate thermal stimuli of the left hind limb. This stimulation elicited blood oxygenation level-dependent (BOLD) signals in the corresponding primary somatosensory cortex (S1) [$P < 0.05$, Gaussian random field (GRF) multiple corrected] (Fig. 5). Regions of interest are described in *SI Appendix*, *Materials and Methods* (*SI Appendix*, Fig. S7). As expected, in the LC group, due to injury to the right thoracic cord, essentially no temperature sensation signals from the left hind limb could be transmitted back to the corresponding S1, and there was no BOLD signal detected (Fig. 5). Compared with the LC group, the NT3 group displayed evident restoration of temperature sensation on BOLD signals, indicating that the de novo regenerated neural tissues are likely functional. As another set of controls, we stimulated the right hind limb to elicit temperature sensation BOLD signals in the left cortex in all three groups to

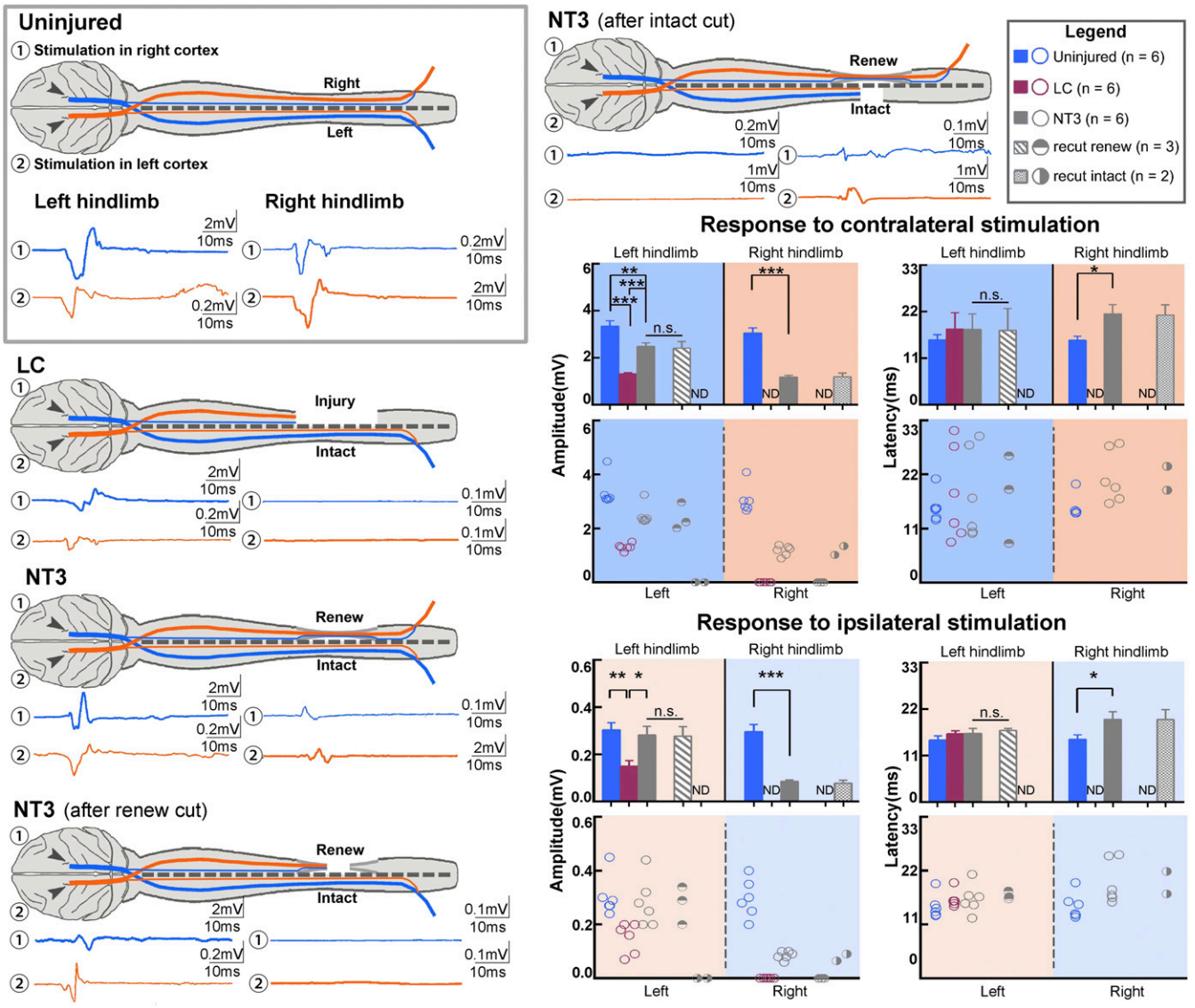

Fig. 4. MEPs demonstrating partial restorations with NT3-chitosan treatment. Stimulation of the right motor cortex evoked MEPs in left anterior tibial muscles (blue), and stimulation of the left motor cortex evoked MEPs in the right hind limb muscles (orange). The relationship between the LC and NT3 groups on MEPs is similar to that on SEPs shown in Fig. 3. Both contralateral (major; thick waveform lines) and ipsilateral (minor; thin waveform lines) responses were analyzed. Quantification and statistical analyses of amplitude and latency period for the aforementioned experiments are shown. Resection results of each animal are also displayed. Technical measurements were repeated twice. Shown are mean ± SEM. $*P < 0.05$, $**P < 0.01$, $***P < 0.001$ by ANOVA or two-tailed independent sample *t* test. See *SI Appendix*, Tables S10 and S11 for exact *n* and *P* values.

demonstrate that the left spinal cords of all three groups of animals were intact and functional (*SI Appendix*, Fig. S7).

Kinematics-Based Analyses Indicating Recovery of Walking Behavior After NT3-Chitosan Treatment. To evaluate potential improvement of animal walking behavior by NT3-chitosan treatment, we used kinematics-based analyses. Monkeys are naturally quadrupedal and, to measure hind limb motor function, we developed bipedal kinematics analyses for monkeys. Monkeys were trained to walk on two legs on a treadmill (Fig. 6*A*). The bipedal gait cycle is composed of a swing phase and a stance phase, which alternate. The bipedal movement of monkeys could initially be elicited by the treadmill; through adaptation, animals could accomplish rhythmic stepping with alternating left and right feet. Kinematics analysis is very sensitive in describing even small abnormalities in animal walking behavior (Fig. 6*B*). We detected the end point trajectory, and found that in the LC group, animals dragged their right legs most of the time (*SI Appendix*, Fig. S8), presenting abnormal stick plots (Fig. 6*C* and Movie S1). In the NT3 group, the animal's right leg demonstrated a successive gait cycle (stepping almost without dragging) (Fig. 6*D* and *SI Appendix*, Fig. S8). We analyzed 127 parameters from kinematics analyses using pairwise correlation and clustering (*SI Appendix*, Fig. S9 and Table S5). Moreover, we selected the 12 clinically most relevant parameters and showed good walking recovery with NT3-chitosan treatment (Fig. 6*E*). Fig. 6*F* demonstrates one complete gait cycle. It was obvious that LC animals' right hind limbs (green) dragged and could not complete a stepping cycle, whereas NT3-chitosan animals demonstrated stepping (Fig. 6*F*). These results strongly indicated that good motor functional recovery was achieved in the NT3 group.

Diffusion Tensor Imaging Analyses Indicating Neural Tissue Regeneration Progress Noninvasively. Magnetic resonance imaging, particularly diffusion tensor imaging (DTI), can be used noninvasively to

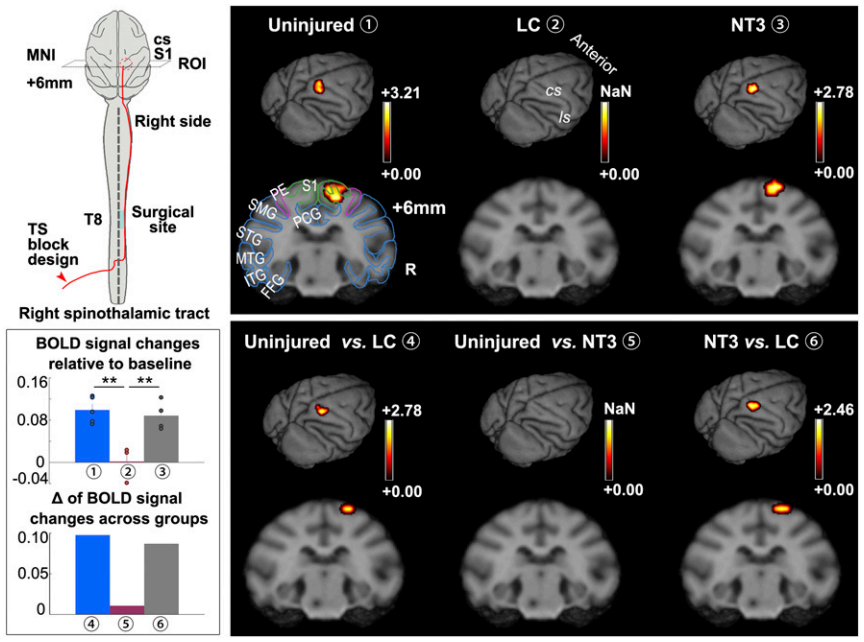

Fig. 5. fMRI analyses indicating recovery of sensory function with NT3-chitosan treatment. Diagram illustrating fMRI experimental design with heat/temperature stimuli applied to the left hind limb. The lateral spinothalamic tract is transmitting the corresponding sensory signal to the somatosensory cortex as illustrated. Averaged fMRI signals within each group were superimposed onto a 3D monkey brain and coronal structural images, respectively ($P < 0.05$, GRF-corrected). Uninjured and NT3 groups displayed significant activation in the S1 area representing the left hind limb receptor field upon thermal stimulation, but LC animals showed no signal. Quantitative BOLD signal changes of the three groups are shown in a bar graph (n = 3 to 5 animals). Intergroup comparisons demonstrate obvious differential activation between the uninjured and LC groups and between the NT3 and LC groups, with no difference between uninjured and NT3 groups (quantitative data are also demonstrated in a bar graph). The schema of brain structures is superimposed onto coronal images. Color scales indicate t values. MNI coordinates are shown. Technical measurements were repeated twice. Error bars represent the mean ± SEM. $^{**}P < 0.01$ by ANOVA. See *SI Appendix*, Tables S10 and S11 for exact n and P values. cs, central sulcus; FFG, fusiform gyrus; ITG, inferior temporal gyrus; ls, lateral sulcus; MNI, Montreal Neurological Coordinates; MTG, middle temporal gyrus; PCG, posterior cingulate cortex; PE, sensory association cortex; R, right; S1, primary somatosensory cortex; SMG, supramarginal gyrus; STG, superior temporal gyrus; T, thoracic vertebra; TS, temperature stimulation; NaN, not a number.

longitudinally track spinal cord neural regeneration progress, which could be an ideal outcome measure for human SCI clinical studies. We used DTI to track spinal cord damage and regeneration in the LC and NT3 groups (Fig. 7*A*). Different colors were used to track the direction of fiber orientations (*SI Appendix*, Fig. S10). In uninjured spinal cords, blue fiber signals filled the whole spinal cord structure in an orderly manner (Fig. 7*B*). After hemitransection and removal of the right thoracic spinal cord segment, the ascending and descending blue fiber tracks were disconnected, leaving a gap on the right side of the spinal cord. The gap persisted 1 y post surgery in lesion controls (Fig. 7*C*). NT3-chitosan treatment led to regeneration based on DTI images 1 y post surgery (Fig. 7*D*). Fractional anisotropy (FA) values and percentage of rostral–caudal voxels of the 2-mm segment at the center of the surgical site demonstrated significant tissue regeneration with NT3-chitosan treatment, while the LC group showed no signs of regeneration (Fig. 7*E*). Longitudinal studies demonstrated that at 2 mo post surgery, in the NT3 group, regenerating blue-colored fiber tracks started to extend into the injury/regeneration regions whereas, for the LC group, no obvious regenerating fiber images were detected (Fig. 7*F*). By 6 mo, ascending and descending fiber tracks merged, and the gap was filled with NT3-chitosan treatment, while the gap (fiber interruption) still persisted in lesion controls. Quantitative analyses of FA values and percentage of rostral–caudal voxels demonstrated significant improvement elicited by NT3-chitosan compared with lesion controls by 6 mo post operation (Fig. 7*G*).

Discussion

We have previously shown that in a rat complete spinal cord transection and extraction model, NT3-chitosan triggered robust de novo neural tissue regeneration and functional recovery (42). Bridging neural structures grown in NT3-chitosan matrix in rats are very similar to those grown in monkeys. In rodents, enhanced neurogenesis from endogenous stem cells and formation of nascent relay neural networks participate in sensory and motor functional recovery, in addition to robust axonal regeneration (42). In monkeys, we also observed what appeared to be neuronal cell bodies in addition to axon bundles in the regenerated tissue. CST labeling experiments demonstrated robust long-distance axonal regeneration, where CSTs grow into the lesion area and also exit the distal boundary and extend into the distal spinal cord. How these newly generated axons manage to reconnect to the correct alpha motor neurons and conduct voluntary movement remain to be determined. Since, in monkeys, we used a spinal cord hemisection, rather than complete transection as in rats, potential contributions/compensations from the left intact cord for the sensory and motor functional recovery become a formal possibility. Resections of intact left cord or regenerated neural cable demonstrated via MEP and SEP that sensory and motor functional recoveries appeared to be dependent on de novo regenerated neural tissues.

To assess whether differences in size of the lesions long-term after the initial surgical procedure may influence motor functional outcomes, we attempted to have a rough assessment of the size of the lesions more than 1 y post operation. We picked middle spinal cord longitudinal sections (serial sections 27, 28, and 29 from 10-μm longitudinal section series) and demarcated the lesion area and speared area, the summation of which gives the total corresponding spinal cord area. We measured each area and calculated the relative lesion area (i.e., lesion area over total corresponding area) (*SI Appendix*, Fig. S11 and Table S6). Subsequently, we performed correlation analyses between the resultant lesion size and 12 clinically relevant kinematics walking parameters (*SI Appendix*, Tables S7–S9) in the LC and NT3 groups separately and in combination. Our conclusion is that there is no positive correlation, suggesting that the smaller the initial or final lesion size the better the walking behavior. It is obvious that the NT3 group has a relatively regular lesion area, while in the LC group the final lesion area is more variable in shape and size. This is likely due to the antiinflammatory function of NT3-chitosan, which inhibited secondary lesions.

In this monkey SCI model, the mode of regeneration is very similar to that of rats (42, 44). We have previously shown in rats that NT3-chitosan is neural-protective, neurogenic, prorevascularizing, and highly antiinflammatory. The antiinflammatory effect of NT3-chitosan also contributed to better regeneration in rodent models (44). In this study, damage to the right spinal cord appeared to influence the function of the left spinal cord, as revealed by reduced SEP and MEP signals. Such influence on the left spinal cord was

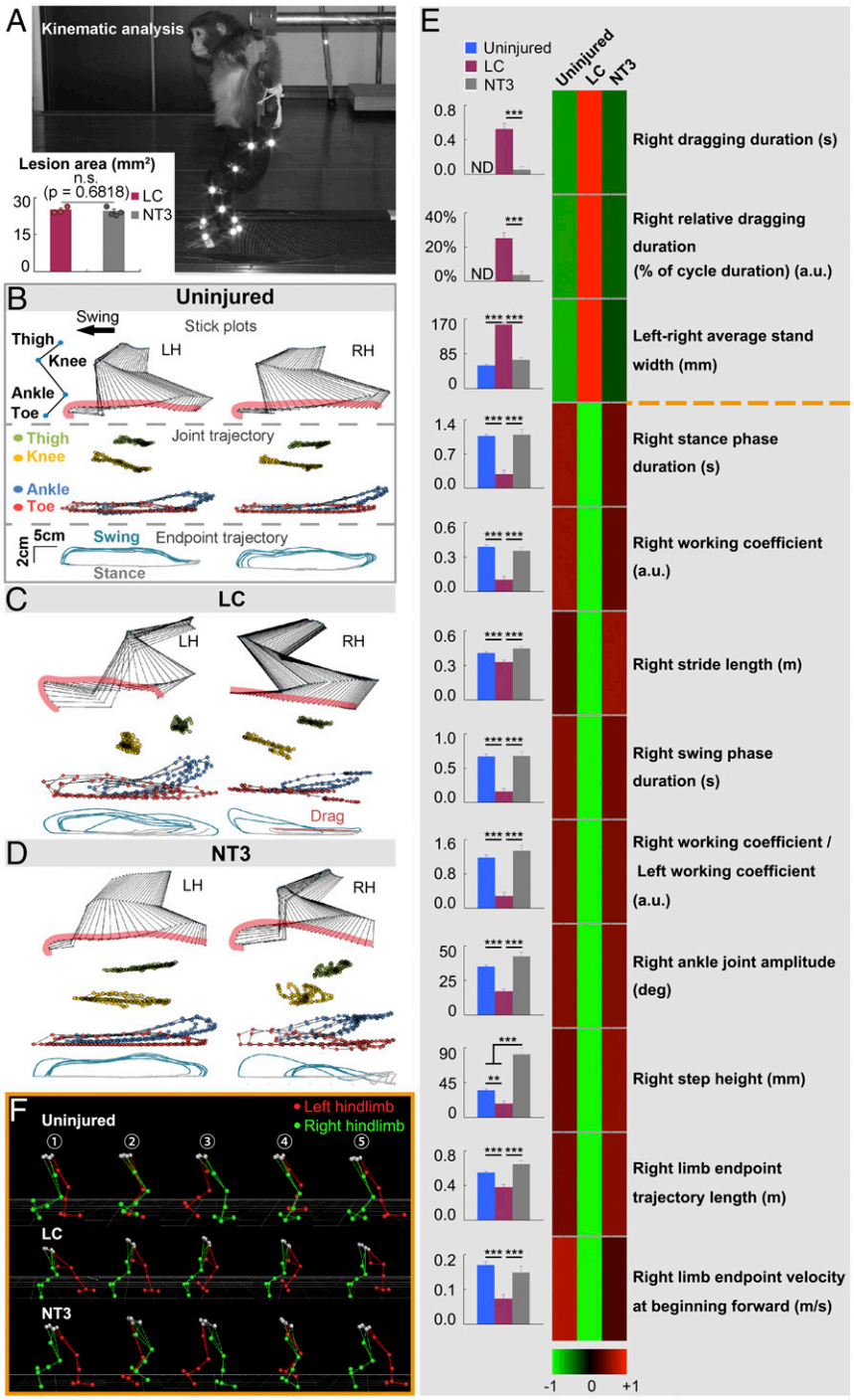

Fig. 6. Improvement of animal walking behavior after NT3-chitosan treatment. (*A*) Lesion areas were similar in size and comparable between the LC and NT3 groups. (*B–D*) Bilateral hind limb kinematics, joint trajectory, and end point trajectory during bipedal locomotion in uninjured (*B*), LC (*C*), and NT3 (*D*) monkeys are displayed. The arrow indicates the direction of stepping (swing phase). Stick figures represent the hind limb (left, LH; right, RH) and precisely describe the animal's stepping movements in the swing. The joint trajectory showed continuous movement of representative joints during stepping. Successive trajectories (gait cycles, 5) of the hind limb end point during stance (gray), swing (blue), and dragging (red) are shown for each condition together. The repeated trajectories were superimposed to show the gait consistency. (*E*) Clustering matrix of 12 clinically relevant gait parameters for three groups of animals is shown. These parameters were chosen to evaluate the overall gait performance. The color scale indicates relative values of each parameter. In the matrix, relative values in the NT3 group are much closer to that of the uninjured group. Raw data are also shown in bar graphs (*Left*) (n = 3 to 5 animals). Technical measurements were repeated at least three times. Shown are mean ± SEM. $^{**}P < 0.01$, $^{***}P < 0.001$ by ANOVA or Kruskal–Wallis test or two-tailed Mann–Whitney U test. See *SI Appendix*, Tables S10 and S11 for exact n and P values. (*F*) Hind limb models displayed a representative gait cycle in uninjured and NT3 monkeys. Step phases of the right hind limb: ① the end of the stance phase; ② mid swing near the vertical line of the body; ③ the end of the swing phase; ④ mid stance with contralateral hind limb (LH) near the vertical line of the body; and ⑤ the end of the stance phase. An LC animal (*Middle*) showed a dragging right hind limb in the whole gait cycle.

attenuated by NT3-chitosan, consistent with the antiinflammatory effect and reduced secondary lesions by the bioactive material. We think additive actions of NT3 and chitosan could be key to success in triggering robust regeneration (44).

This study using nonhuman primates represents a substantial advancement in translating our initial study using rodents to human therapy. Moreover, fMRI and kinematics walking analyses, as well as DTI, though not necessarily reflecting the actual volume of axonal fiber bundles (45), are all noninvasive ways of effectively assessing regeneration and functional recovery over time, and can be used with humans. While we do acknowledge that the hemitransection model is different from most SCI cases in humans (26), our findings here are significant because the previously reported three actions of NT3-chitosan, namely (*i*) neuroprotection and neurogenesis, (*ii*) prorevascularization, and (*iii*) antiinflammation, should allow for its application in a variety of SCI conditions. Particularly given that an injectable NT3-chitosan material has been manufactured (46), the versatile nature of the injectable material may warrant its usage in contusion or crush injury conditions. We also realize that the medical community is interested in not only treating acute injury but also chronic injury. While this study is mainly focused on acute injury repair, we hypothesize that for treatment of chronic injury, removal or at least partial removal of glial scar tissue will be needed to not

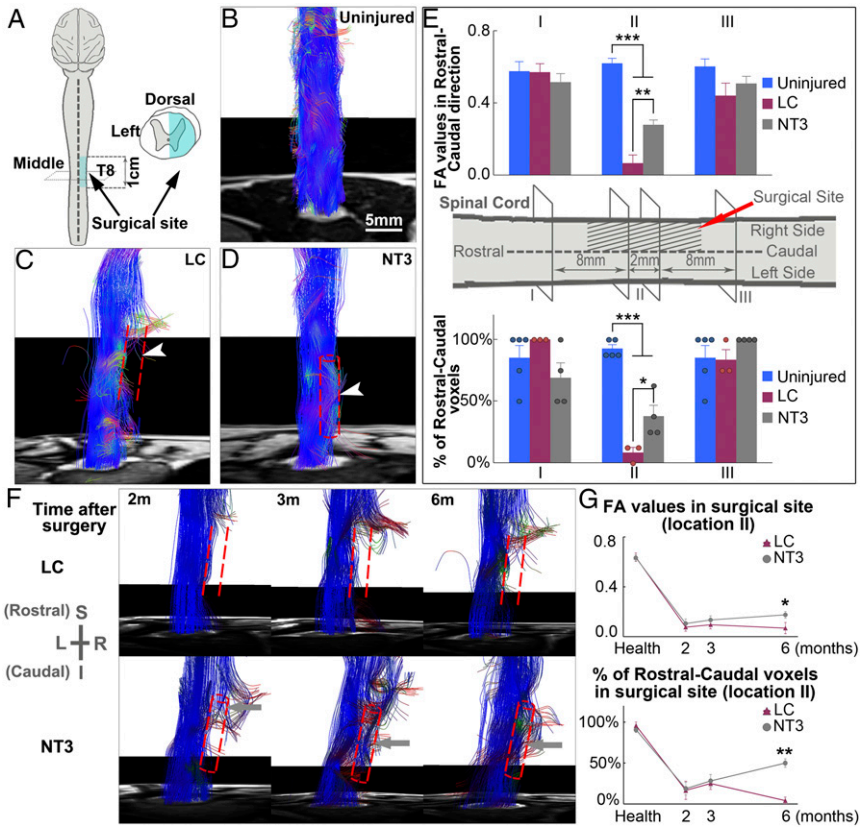

Fig. 7. MRI results indicating NT3-chitosan enabled neural tissue regeneration after SCI. (*A*) Diagram illustrating the spinal cord hemisection and extraction model. (*B–D*) Typical fiber tract reconstruction for the uninjured (*B*), LC (*C*), and NT3 (*D*) groups is displayed. In the LC group, fiber tracts were interrupted, deformed, and distorted at the border rostral and caudal to the lesion, with no fiber tracts present within the lesion (*C*). In contrast, in the NT3 group, numerous regenerated fiber tracts extend across the surgical site, reconnecting the rostral and caudal ends of the injured cord (*D*). Arrowheads indicate the surgical sites. Red dashed lines indicate the damaged zone, and tubular structures in the NT3 group represent positions of chitosan tubes. (*E*) Graph of averaged FA values and percentages of rostral–caudal voxel numbers of the three groups in three locations (I to III). Results of two levels in the middle site were gathered as location II. The NT3 group showed significantly higher FA values and percentages of voxels compared with the LC group ($n = 3$ to 5 animals). (*F*) Diffusion tensor fiber tracking tractography showed longitudinal changes of lesion (*Top*) and treated (*Bottom*) spinal cord with time after operation. LC animals showed a lack of neural fibers in the damaged zone, while NT3 animals displayed regenerated fiber bundle growth progressively with time and eventually connecting the two ends of the severed cord at 6 mo. I, inferior; L, left; R, right; S, superior. (*G*) Time courses of changes in FA values and percentages of rostral–caudal voxels at the center of the surgical site (location II) from LC and NT3 groups up to 6 mo post operation ($n = 3$ or 4 animals). Technical measurements were repeated twice. Shown are mean ± SEM. $^*P < 0.05$, $^{**}P < 0.01$, $^{***}P < 0.001$ by ANOVA or two-tailed independent sample *t* test or two-tailed Mann–Whitney *U* test. See *SI Appendix*, Tables S10 and S11 for exact *n* and *P* values.

only elicit fresh lesion responses but also to create a physical space for transplanting the NT3-chitosan tube. With this, long-distance axonal regeneration could be induced within an optimal neurotrophic and antiinflammatory microenvironment. Of course, studies using NT3-chitosan to repair chronic lesion models using NHPs are currently ongoing. To achieve functional recovery, long-distance axonal regeneration must be coupled with new synapse formation and neural circuitry remodeling. Detailed circuitry mapping will be required in the near future to reveal the logic of neuronal wiring (connectivity) during regeneration. Moreover, as rehabilitation is likely among the most effective clinical means of eliciting neural plasticity and engaging circuitry wiring and pruning, it should be indispensable for good functional recovery after SCI.

Taken together, this study using NHPs represents an important milestone, paving the way to clinical studies using NT3-chitosan for SCI treatment.

Materials and Methods

NT3-Chitosan Tube Fabrication. The chitosan tube was fabricated by the method previously published (41, 42, 47). For detailed methods, see *SI Appendix, Materials and Methods*.

Animal Models. Thirty-eight female rhesus monkeys (*Macaca mulatta*, 4 to 6 y old), each weighing 5 ± 1 kg, were used for these experiments. All surgical and experimental procedures in monkeys were approved by and performed in accordance with the standards of the Experimental Animal Center of Capital Medical University and the Beijing Experimental Animal Association. Details are provided in *SI Appendix, Materials and Methods*.

Immunohistochemistry/Fluorescence Staining. Morphological analysis was performed as detailed in *SI Appendix, Materials and Methods*.

Light and Electron Microscopies. These observations were performed as detailed in *SI Appendix, Materials and Methods*.

BDA Tracing. This observation was performed as detailed in *SI Appendix, Materials and Methods*.

SEP and MEP Examination. Electrophysiological study was carried out for each group ($n = 6$ animals). For detailed information, see *SI Appendix, Materials and Methods*.

Anesthesia for MRI Examinations. Animals of each group ($n = 3$ to 5 animals) were anesthetized for MRI scanning. For detailed information, see *SI Appendix, Materials and Methods*.

fMRI Stimulation. Innocuous heat stimulation was used for the fMRI somatosensory test. For detailed information, see *SI Appendix, Materials and Methods*.

MRI Data Acquisition. All MRI research was accomplished with the Siemens 3T MRI instrument. Detailed scanning parameters are provided in *SI Appendix, Materials and Methods*.

fMRI Data Processing. All fMRI data were processed with Statistical Parametric Mapping (SPM) version 8 (www.fil.ion.ucl.ac.uk/spm/). For detailed processes, see *SI Appendix, Materials and Methods*.

DTI Data Processing. DTI scans were processed and analyzed by means of dedicated MedINRIA software (www-sop.inria.fr/asclepios/software/MedINRIA). For detailed processes, see *SI Appendix, Materials and Methods*.

Kinematics Analyses of Bipedal Locomotion. The bipedal locomotion of the animals was characterized by gait test. More details are provided in *SI Appendix, Materials and Methods*.

Statistical Analyses. Standard statistical tests were used to analyze the data. Please see *SI Appendix, Materials and Methods* for further information.

ACKNOWLEDGMENTS. We thank Drs. Michael V. Sofroniew, Vance Lemmon, and Mark Tuszynski for their advice and academic assistance. We thank technicians in the Core Facility Center of Capital Medical University, Beijing MRI Center for Brain Research, and National Research Center for Rehabilitation Technical Aids for furnishing technical expertise. This work was supported by the National Natural Science Foundation of China (Grants 31730030, 31650001, 31670988, 31771053, 31320103903, 31620103904, 81330030, 81650110524, and 31730039), Ministry of Science and Technology of China (Grants 2017YFC1104001, 2017YFC1104002, 2016YFA0100801, and 2015CB351701), Beijing Science and Technology Program (Grants Z171100002217066 and Z181100001818007), Beijing Natural Science Foundation Program (Grant KZ201810025030), and Chinese Academy of Sciences (Grant ZDYZ2015-2). The work is also supported by the National Institutes of Health (NIH5R21NS095184-02) and "RNAseq on Single Cell and Beyond Core" in the Developmental Disabilities Research Center (NIH5U54HD087101-02) at the University of California, Los Angeles.

1. David S, Lacroix S (2003) Molecular approaches to spinal cord repair. *Annu Rev Neurosci* 26:411–440.
2. Domeniconi M, et al. (2002) Myelin-associated glycoprotein interacts with the Nogo66 receptor to inhibit neurite outgrowth. *Neuron* 35:283–290.
3. Schwab ME (2004) Nogo and axon regeneration. *Curr Opin Neurobiol* 14:118–124.
4. Sivasankaran R, et al. (2004) PKC mediates inhibitory effects of myelin and chondroitin sulfate proteoglycans on axonal regeneration. *Nat Neurosci* 7:261–268.
5. Andrews EM, Richards RJ, Yin FQ, Viapiano MS, Jakeman LB (2012) Alterations in chondroitin sulfate proteoglycan expression occur both at and far from the site of spinal contusion injury. *Exp Neurol* 235:174–187.
6. Mabon PJ, Weaver LC, Dekaban GA (2000) Inhibition of monocyte/macrophage migration to a spinal cord injury site by an antibody to the integrin alphaD: A potential new anti-inflammatory treatment. *Exp Neurol* 166:52–64.
7. Silva NA, Sousa N, Reis RL, Salgado AJ (2014) From basics to clinical: A comprehensive review on spinal cord injury. *Prog Neurobiol* 114:25–57.
8. Johnson PJ, Tatara A, Shiu A, Sakiyama-Elbert SE (2010) Controlled release of neurotrophin-3 and platelet-derived growth factor from fibrin scaffolds containing neural progenitor cells enhances survival and differentiation into neurons in a subacute model of SCI. *Cell Transplant* 19:89–101.
9. Elliott Donaghue I, Tator CH, Shoichet MS (2016) Local delivery of neurotrophin-3 and anti-NogoA promotes repair after spinal cord injury. *Tissue Eng Part A* 22:733–741.
10. Yang Z, Duan H, Mo L, Qiao H, Li X (2010) The effect of the dosage of NT-3/chitosan carriers on the proliferation and differentiation of neural stem cells. *Biomaterials* 31:4846–4854.
11. Yang Z, Qiao H, Sun Z, Li X (2013) Effect of BDNF-plasma-collagen matrix controlled delivery system on the behavior of adult rats neural stem cells. *J Biomed Mater Res A* 101:599–606.
12. Ishii K, et al. (2006) Neutralization of ciliary neurotrophic factor reduces astrocyte production from transplanted neural stem cells and promotes regeneration of corticospinal tract fibers in spinal cord injury. *J Neurosci Res* 84:1669–1681.
13. Liang P, Jin LH, Liang T, Liu EZ, Zhao SG (2006) Human neural stem cells promote corticospinal axons regeneration and synapse reformation in injured spinal cord of rats. *Chin Med J (Engl)* 119:1331–1338.
14. Chen A, Xu XM, Kleitman N, Bunge MB (1996) Methylprednisolone administration improves axonal regeneration into Schwann cell grafts in transected adult rat thoracic spinal cord. *Exp Neurol* 138:261–276.
15. Guest JD, Rao A, Olson L, Bunge MB, Bunge RP (1997) The ability of human Schwann cell grafts to promote regeneration in the transected nude rat spinal cord. *Exp Neurol* 148:502–522.
16. Lee YS, Hsiao I, Lin VW (2002) Peripheral nerve grafts and aFGF restore partial hindlimb function in adult paraplegic rats. *J Neurotrauma* 19:1203–1216.
17. Nordblom J, Persson JKE, Svensson M, Mattsson P (2009) Peripheral nerve grafts in a spinal cord prosthesis result in regeneration and motor evoked potentials following spinal cord resection. *Restor Neurol Neurosci* 27:285–295.
18. Bradbury EJ, et al. (2002) Chondroitinase ABC promotes functional recovery after spinal cord injury. *Nature* 416:636–640.
19. Pakulska MM, Vulic K, Shoichet MS (2013) Affinity-based release of chondroitinase ABC from a modified methylcellulose hydrogel. *J Control Release* 171:11–16.
20. Shen Y, et al. (2009) PTPsigma is a receptor for chondroitin sulfate proteoglycan, an inhibitor of neural regeneration. *Science* 326:592–596.
21. Guest JD, et al. (2008) Xenografts of expanded primate olfactory ensheathing glia support transient behavioral recovery that is independent of serotonergic or corticospinal axonal regeneration in nude rats following spinal cord transection. *Exp Neurol* 212:261–274.
22. Li X, Yang Z, Zhang A (2009a) The effect of neurotrophin-3/chitosan carriers on the proliferation and differentiation of neural stem cells. *Biomaterials* 30:4978–4985.
23. Li X, Yang Z, Yang Y (2006) Morphological and electrophysiological evidence for regeneration of transected spinal cord fibers and restoration of motor functions in adult rats. *Chin Sci Bull* 51:918–926.
24. Nomura H, et al. (2008) Delayed implantation of intramedullary chitosan channels containing nerve grafts promotes extensive axonal regeneration after spinal cord injury. *Neurosurgery* 63:127–141, discussion 141–143.
25. Mestas J, Hughes CCW (2004) Of mice and not men: Differences between mouse and human immunology. *J Immunol* 172:2731–2738.
26. Courtine G, et al. (2007) Can experiments in nonhuman primates expedite the translation of treatments for spinal cord injury in humans? *Nat Med* 13:561–566.
27. Courtine G, et al. (2005) Performance of locomotion and foot grasping following a unilateral thoracic corticospinal tract lesion in monkeys (*Macaca mulatta*). *Brain* 128:2338–2358.
28. Nishimura Y, et al. (2007) Time-dependent central compensatory mechanisms of finger dexterity after spinal cord injury. *Science* 318:1150–1155.
29. Rosenzweig ES, et al. (2010) Extensive spontaneous plasticity of corticospinal projections after primate spinal cord injury. *Nat Neurosci* 13:1505–1510.
30. Vessal M, Aycock A, Garton MT, Ciferri M, Darian-Smith C (2007) Adult neurogenesis in primate and rodent spinal cord: Comparing a cervical dorsal rhizotomy with a dorsal column transection. *Eur J Neurosci* 26:2777–2794.
31. Wannier T, Schmidlin E, Bloch J, Rouiller EM (2005) A unilateral section of the corticospinal tract at cervical level in primate does not lead to measurable cell loss in motor cortex. *J Neurotrauma* 22:703–717.
32. Albin MS, White RJ, Acosta-Rua G, Yashon D (1968) Study of functional recovery produced by delayed localized cooling after spinal cord injury in primates. *J Neurosurg* 29:113–120.
33. Kitamura K, et al. (2011) Human hepatocyte growth factor promotes functional recovery in primates after spinal cord injury. *PLoS One* 6:e27706.
34. Beaud ML, et al. (2008) Anti-Nogo-A antibody treatment does not prevent cell body shrinkage in the motor cortex in adult monkeys subjected to unilateral cervical cord lesion. *BMC Neurosci* 9:5.
35. Freund P, et al. (2006) Nogo-A-specific antibody treatment enhances sprouting and functional recovery after cervical lesion in adult primates. *Nat Med* 12:790–792.
36. Freund P, et al. (2007) Anti-Nogo-A antibody treatment enhances sprouting of corticospinal axons rostral to a unilateral cervical spinal cord lesion in adult macaque monkey. *J Comp Neurol* 502:644–659.
37. Iwanami A, et al. (2005) Transplantation of human neural stem cells for spinal cord injury in primates. *J Neurosci Res* 80:182–190.
38. Kobayashi Y, et al. (2012) Pre-evaluated safe human iPSC-derived neural stem cells promote functional recovery after spinal cord injury in common marmoset without tumorigenicity. *PLoS One* 7:e52787.
39. Levi ADO, et al. (2002) Peripheral nerve grafts promoting central nervous system regeneration after spinal cord injury in the primate. *J Neurosurg* 96(2, Suppl):197–205.
40. Pritchard CD, et al. (2010) Establishing a model spinal cord injury in the African green monkey for the preclinical evaluation of biodegradable polymer scaffolds seeded with human neural stem cells. *J Neurosci Methods* 188:258–269.
41. Li X, Yang Z, Zhang A, Wang T, Chen W (2009b) Repair of thoracic spinal cord injury by chitosan tube implantation in adult rats. *Biomaterials* 30:1121–1132.
42. Yang Z, et al. (2015) NT3-chitosan elicits robust endogenous neurogenesis to enable functional recovery after spinal cord injury. *Proc Natl Acad Sci USA* 112:13354–13359.
43. Piedras MJGM, Hernández-Laín A, Cavada C (2011) Clinical care and evolution of paraplegic monkeys (*Macaca mulatta*) over fourteen months post-lesion. *Neurosci Res* 69:135–143.
44. Duan H, et al. (2015) Transcriptome analyses reveal molecular mechanisms underlying functional recovery after spinal cord injury. *Proc Natl Acad Sci USA* 112:13360–13365.
45. Fujiyoshi K, et al. (2007) In vivo tracing of neural tracts in the intact and injured spinal cord of marmosets by diffusion tensor tractography. *J Neurosci* 27:11991–11998.
46. Mo L, Yang Z, Zhang A, Li X (2010) The repair of the injured adult rat hippocampus with NT-3-chitosan carriers. *Biomaterials* 31:2184–2192.
47. Yang Z, Mo L, Duan H, Li X (2010) Effects of chitosan/collagen substrates on the behavior of rat neural stem cells. *Sci China Life Sci* 53:215–222.